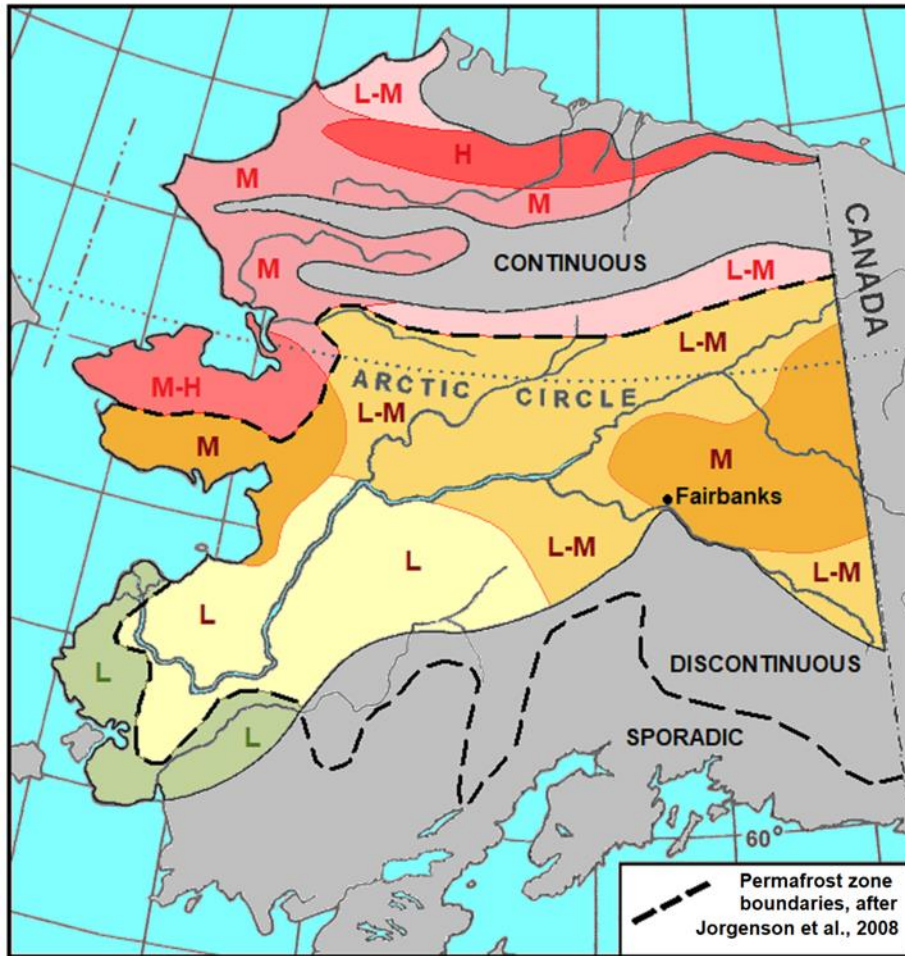


Supplementary Material - Figures



Yedoma occurrence:

	Low (L)	Medium (M)	High (H)		
Continuous Permafrost		L-M	M	M-H	H
Discontinuous Permafrost	L	L-M	M		
Sporadic Permafrost	L				

Figure S1. Yedoma occurrence in Alaska within different permafrost zones (Shur et al., 2021a, modified from Kanevskiy et al., 2011, 2016). Data for the map combine our field observations in different parts of Alaska, an analysis of satellite and aerial imagery, and an analysis of published sources.

Right Wall

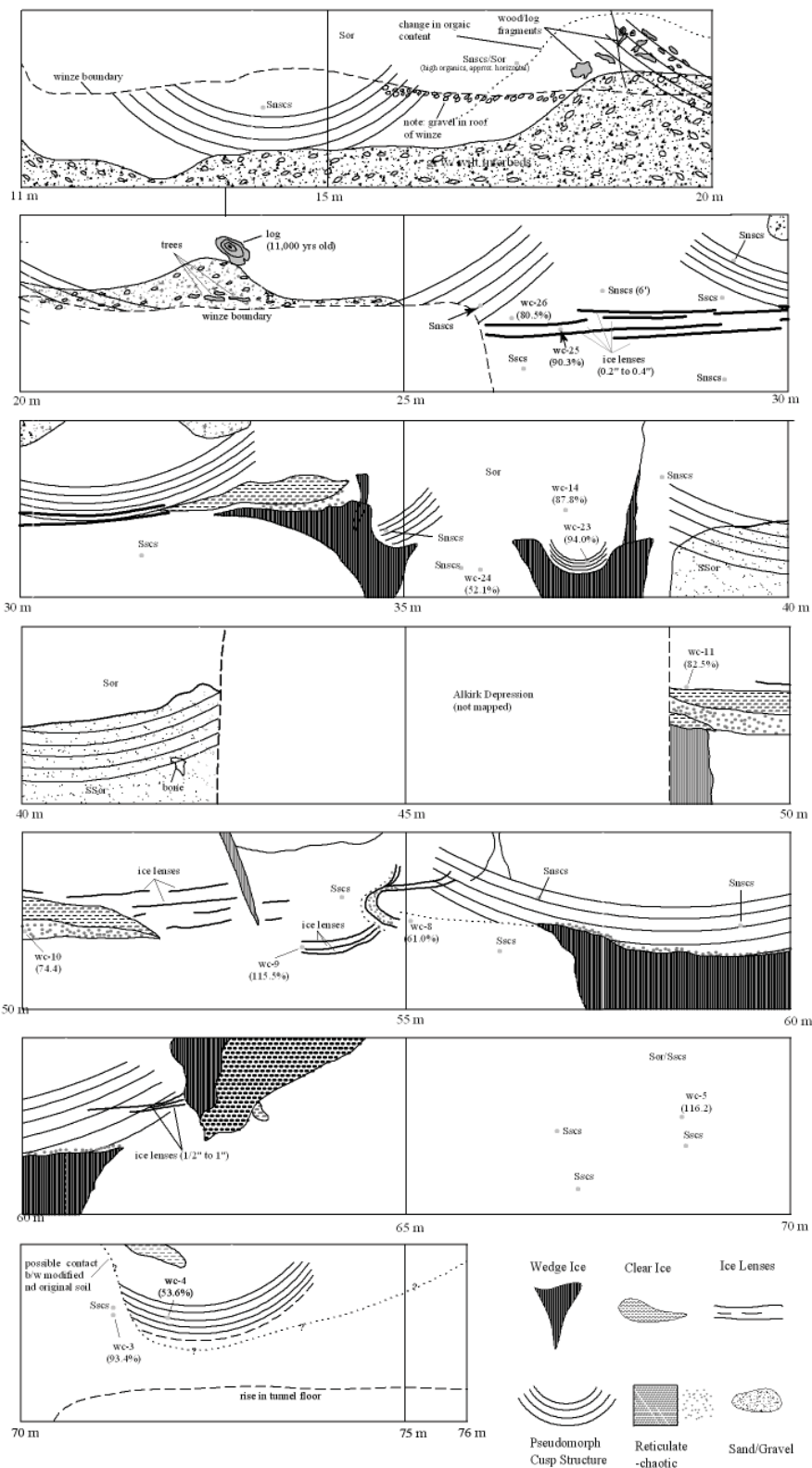


Figure S3. Cryostratigraphic map of part of the main adit of the old CRREL permafrost tunnel (T1), right side (viewed from entrance) of the tunnel (Bray et al, 2006).

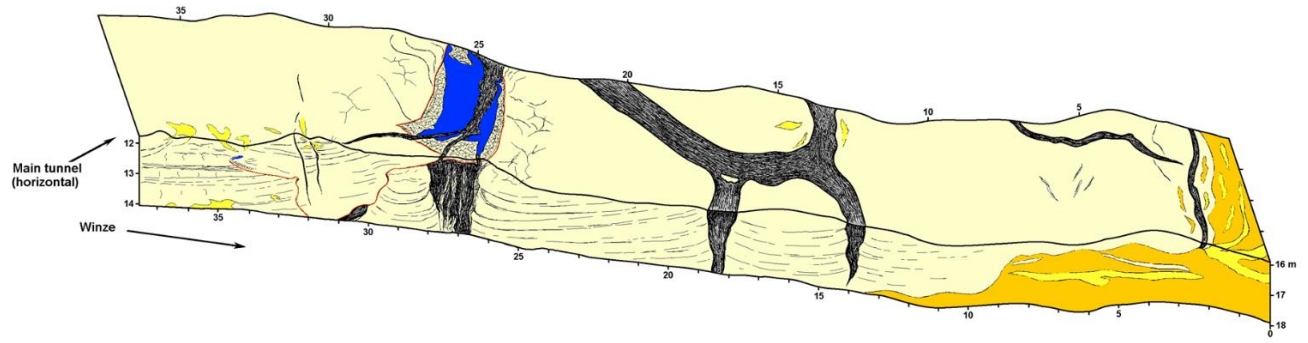


Figure S4. General view of the left wall and the ceiling of the winze (W) of the old CRREL permafrost tunnel (modified from Kanevskiy et al., 2008). For the legend, see **Figure S7**.

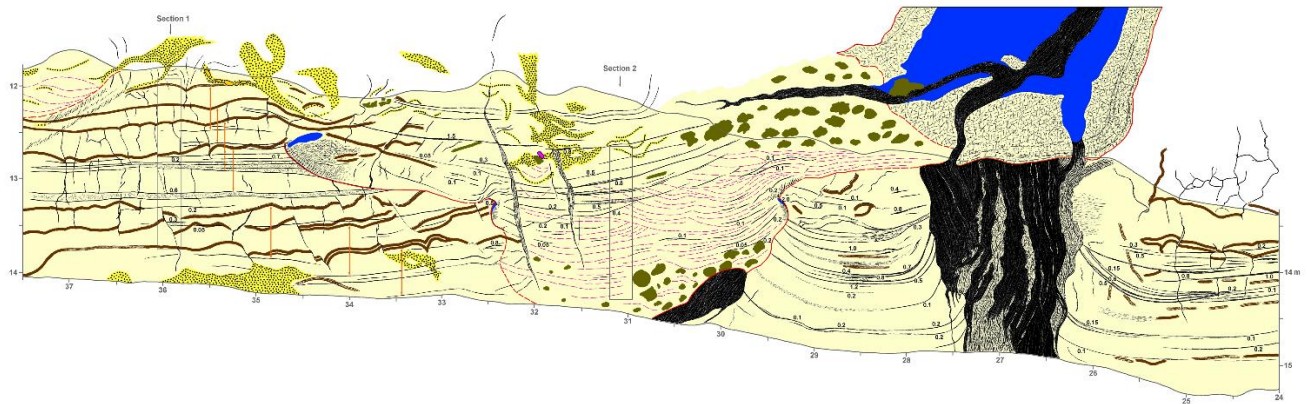


Figure S5. Cryostratigraphic map of the left wall of the winze (W) of the old CRREL permafrost tunnel, distance 24–37 m (modified from Kanevskiy et al., 2008). For the legend, see **Figure S7**.

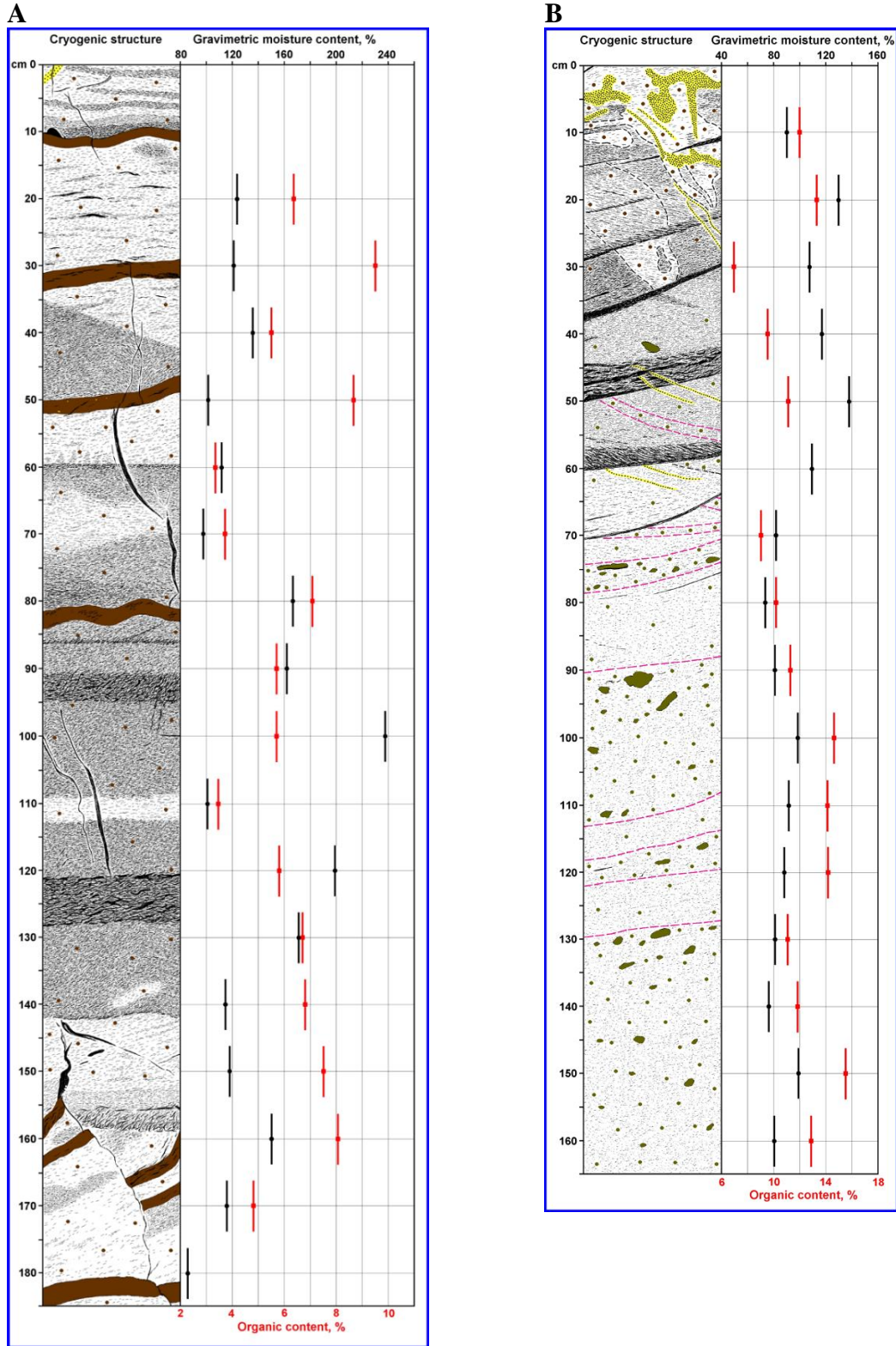


Figure S6. Cryostratigraphy and properties of Sections 1 (A) and 2 (B) of the left wall of the winze (W) of the old CRREL permafrost tunnel; ice is black (modified from Kanevskiy et al., 2008a). Location of these sections is shown in **Figure S5**. For the legend, see **Figure S7**.

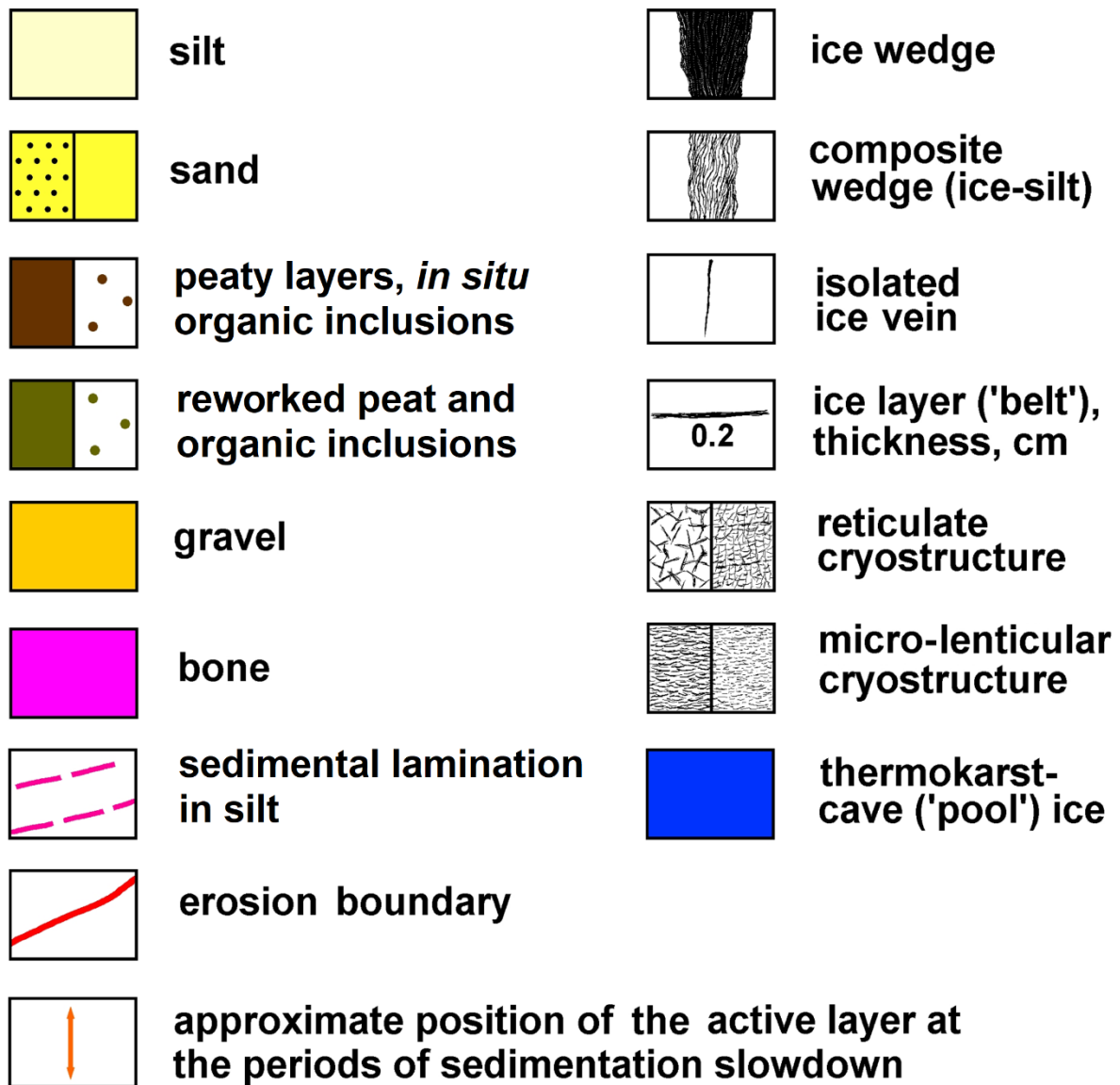


Figure S7. Legend to **Figures S4, S5, and S6** (modified from Kanevskiy et al., 2008).



Figure S8. Photograph of the reticulate-chaotic cryostructure (the handle of the knife is about 6 cm long) (Fortier et al., 2008).

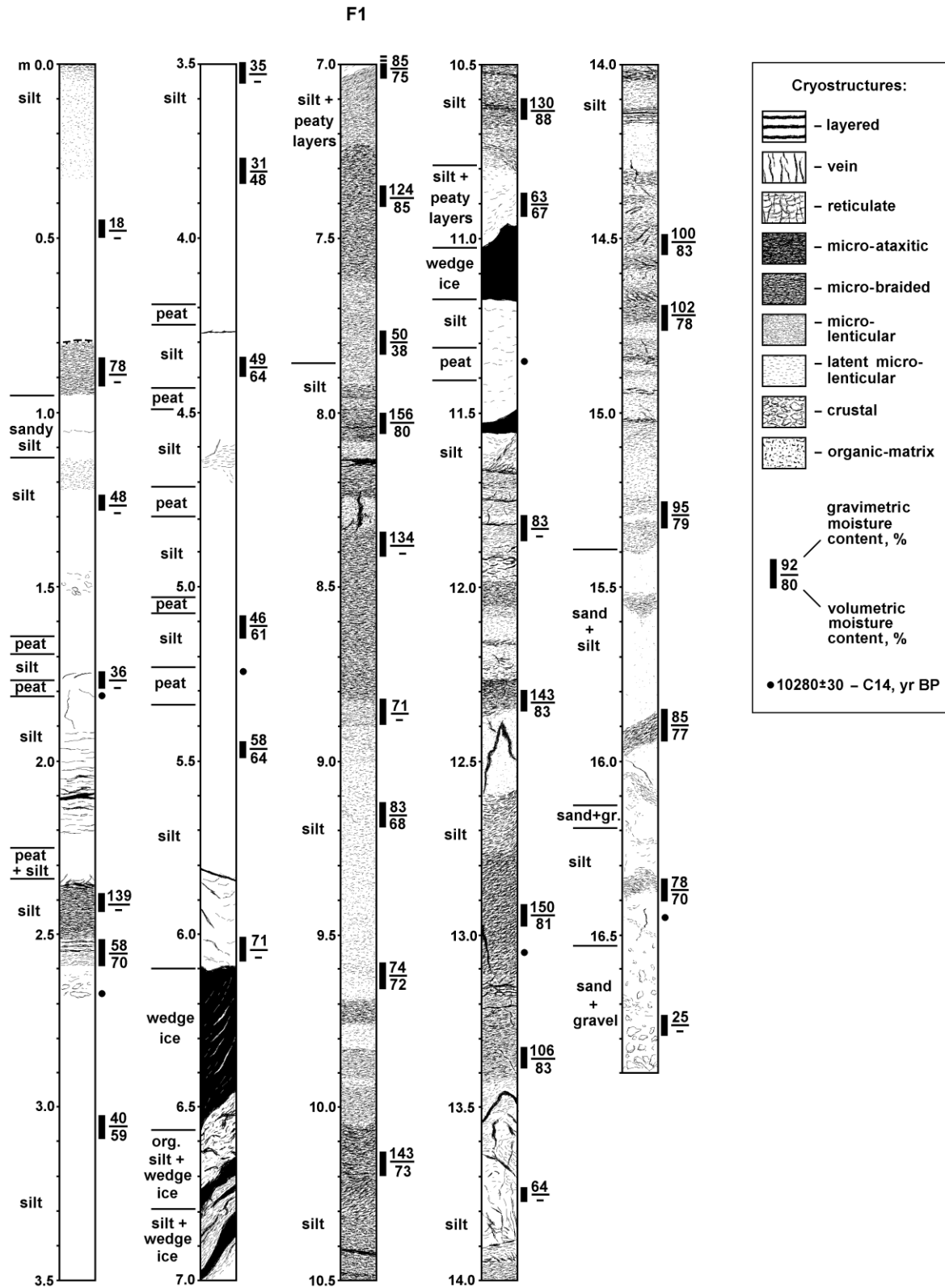


Figure S9. Cryostratigraphy (ice is black) and ice contents of frozen soil, borehole F1, elevation 239.9 m.

F2

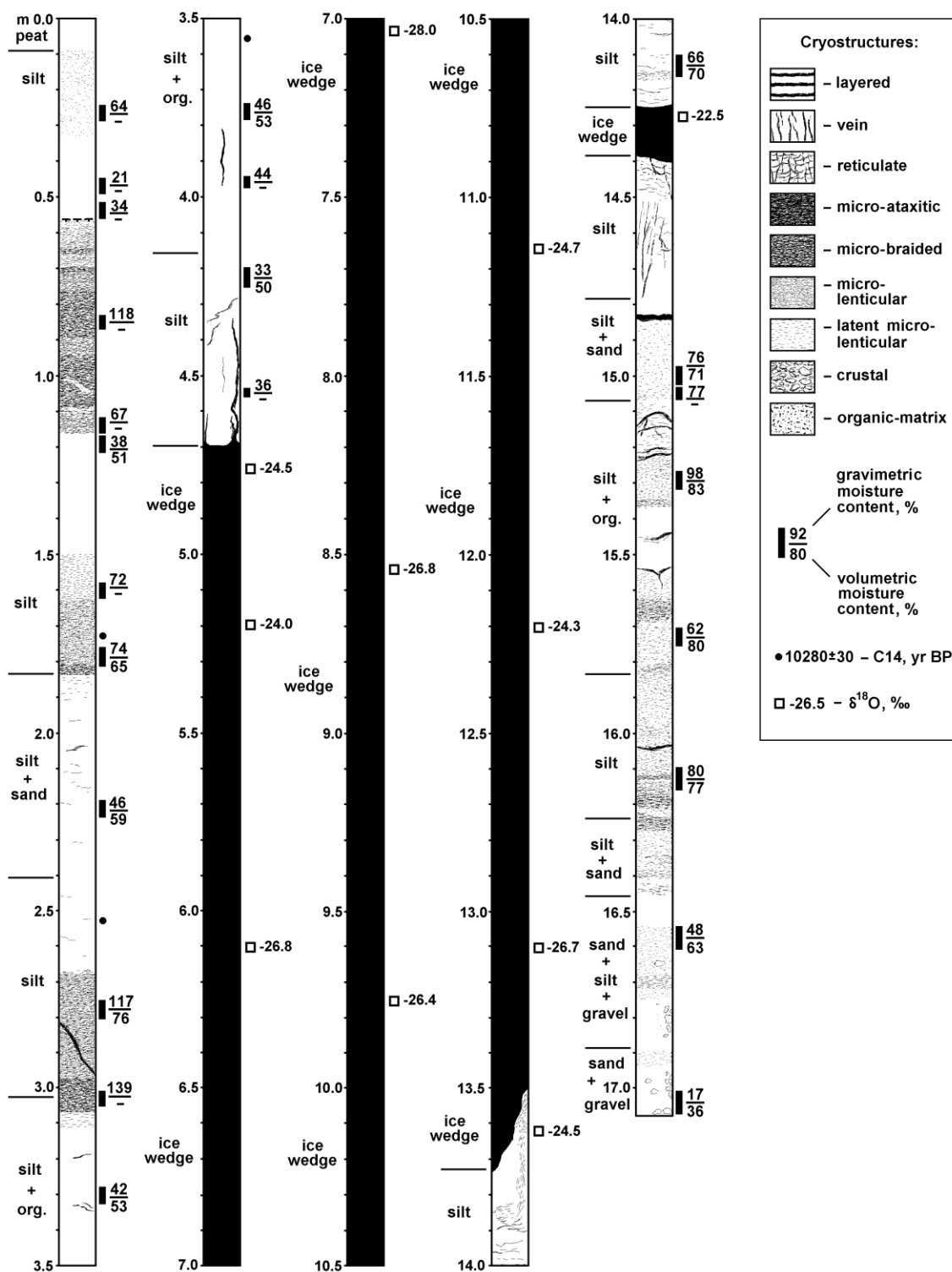


Figure S10. Cryostratigraphy (ice is black) and ice contents of frozen soil, borehole F2, elevation 243.6 m.

F3

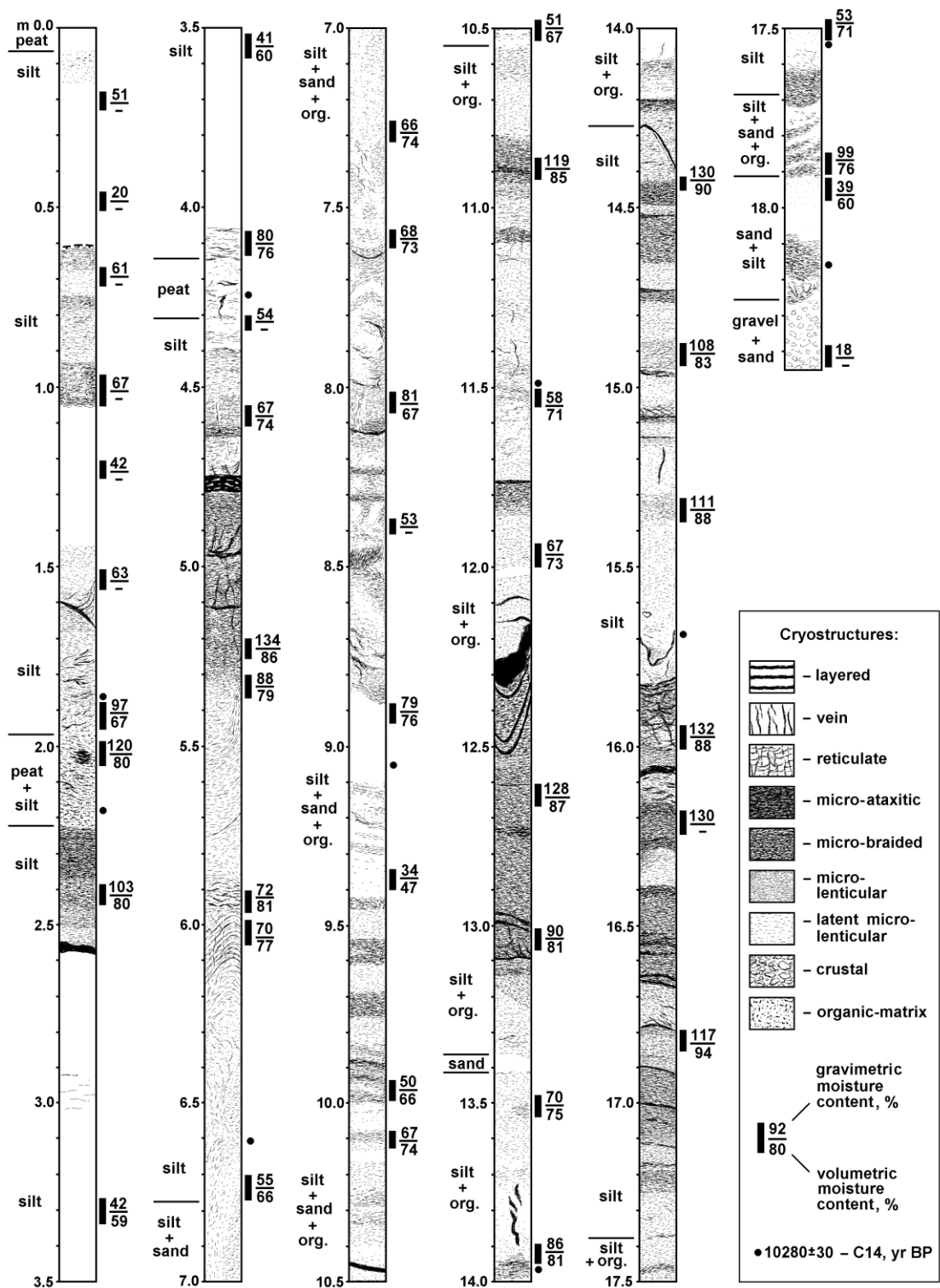


Figure S11. Cryostratigraphy (ice is black) and ice contents of frozen soil, borehole F3, elevation 241.6 m.

F4

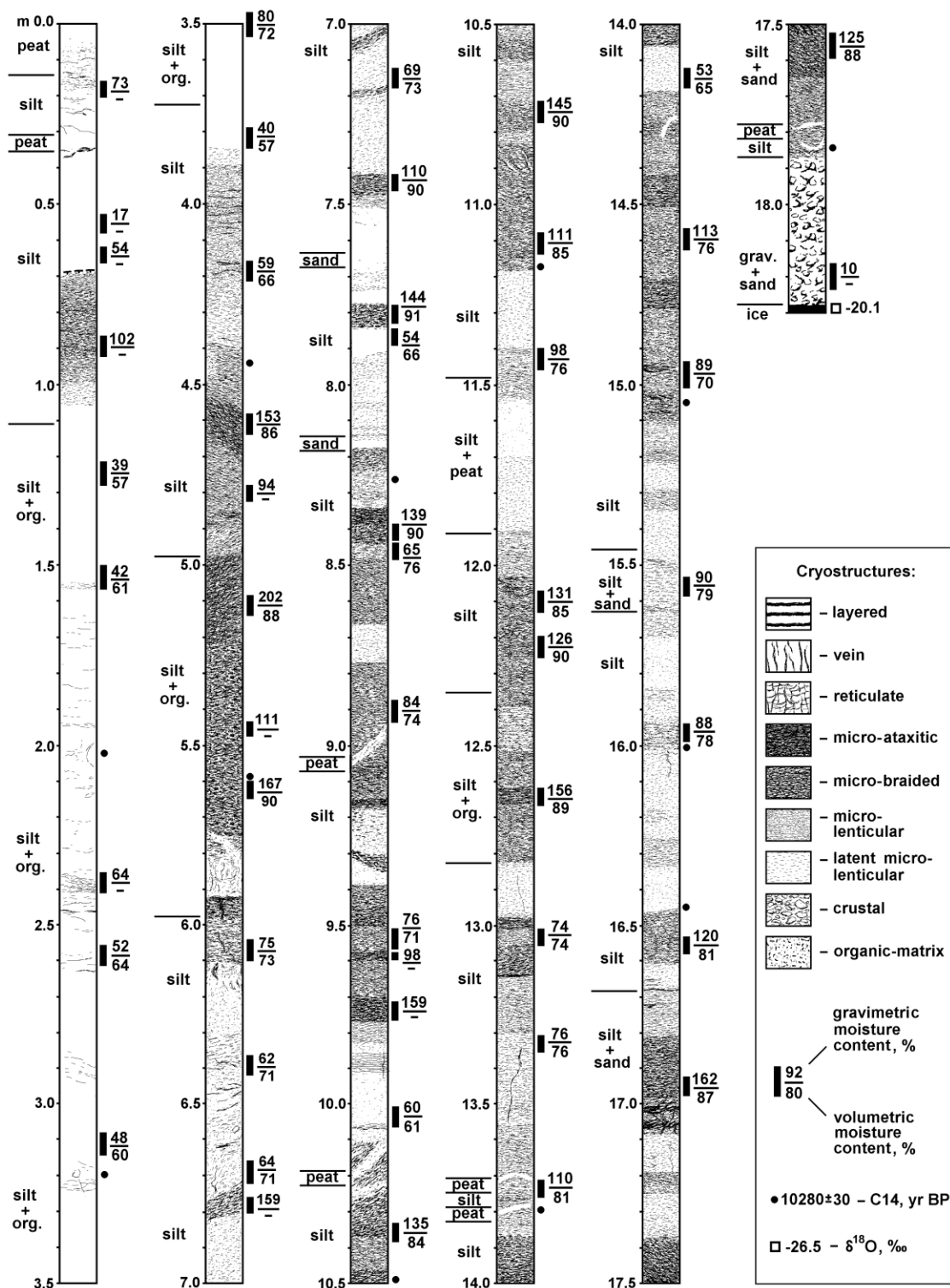


Figure S12. Cryostratigraphy (ice is black) and ice contents of frozen soil, borehole F4, elevation 243.6 m.



Figure S13. Small ice wedge in syngenetically frozen silt; note peat layers and numerous inclusions of organic matter. Left wall of the main adit of the new tunnel (T2), distance 23.0-27.0 m, elevation 229.2-231.5 m (for location, see **Figure 6**).



Figure S14. Large late Pleistocene ice wedge and several smaller ones of presumably Holocene age, visible on the ceiling and the upper part of the tunnel wall. Right wall of the main adit of the new tunnel (T2), distance 31.6-35.3 m, elevation 229.8-232.0 m (for location, see **Figures 6 and 7**).



Figure S15. Large Late Pleistocene ice wedge and deformed peat layers. Left wall of the main adit of the new tunnel (T2), distance 31.0-33.5 m, elevation 228.7-230.6 m (for location, see **Figure 6**).



Figure S16. Large body of thermokarst-cave ice. Right wall of the main adit of the new tunnel (T2), distance 39.7-42.8 m, elevation 228.9-231.5 m (for location and interpretation, see **Figures 6 and 7**; for details, see **Figures S17, S18, and S19**).



Figure S17. Thermokarst-cave ice (see **Figure S16**) underlain by silt with reticulate-chaotic cryostructure; note the presence of woody debris in the silt at the bottom of the thermokarst-cave ice body. Right wall of the main adit of the new tunnel (T2), distance 41.8-42.5 m, elevation 229.2-229.6 m (for location, see **Figures 6 and 7**).



Figure S18. Thermokarst-cave ice (see **Figure S16**); horizontal stratification and suspended wood fragments indicate several stages of water accumulation and thermokarst-cave ice aggradation in the underground cavity. Right wall of the main adit of the new tunnel (T2), distance 38.9-39.9 m, elevation 229.0-229.9 m (for location, see **Figures 6 and 7**).



Figure S19. Stratified and cross-stratified silt and silty sand with numerous inclusions of the organic matter reworked by fluvial processes; note thermokarst-cave ice at the bottom (see **Figure S18**); the boundary between stratified sediments and massive ice may be interpreted as an erosion unconformity. Right wall of the main adit of the new tunnel (T2), distance 38.6-39.1 m, elevation 229.5-229.9 m (for location, see **Figures 6 and 7**).



Figure S20. Ice wedge surrounded by individual ice veins forming composite (ice/silt) wedge; note a dark-brown layer of buried peat. Right wall of the main adit of the new tunnel (T2), distance 32.8-33.4 m, elevation 229.0-229.5 m (for location, see **Figures 6 and 7**).



Figure S21. Ice wedge truncated by thermal erosion; bodies of thermokarst-cave ice were crossed by the ice wedge of younger generation. Left wall of the main adit of the new tunnel (T2), distance 66.0-70.8 m, elevation 228.7-231.6 m (for location and interpretation, see **Figure 6**).



Figure S22. Ice wedge (with a layer of thermokarst-cave ice on top) truncated by thermokarst; the triangular massive ice body consists of the ice-wedge remnant and thermokarst-cave ice. Left wall of the main adit of the new tunnel (T2), distance 77.2-81.3 m, elevation 228.3-231.2 m (for location and interpretation, see **Figure 6**).



Figure S23. Ice wedge cut by underground thermal erosion and containing thermokarst-cave ice body underlain by ice-rich silt with reticulate-chaotic cryostructure. Right wall of the main adit of the new tunnel (T2), distance 65.2-69.6 m, elevation 227.8-231.6 m (for location and interpretation, see **Figure 6**).



Figure S24. Ice wedge cut by underground thermal erosion; thermokarst-cave ice body and ice-rich silt that formed in the underground cavity were subsequently crossed by the ice wedge of younger generation. Left wall of the main adit of the new tunnel (T2), distance 89.0-93.9 m, elevation 228.2-231.0 m (for location and interpretation, see **Figure 6**).



Figure S25. Layers of gravel and gravelly sand enclosed in Yedoma silt that were penetrated by 0.2- to 0.5-m-wide ice wedges. Layers of gravelly soils probably accumulated in thermo-erosional gullies. Note well-developed horizontal parts of ice wedges that are parallel to the gravel layers (for details, see **Figure S26**). Left wall of the main adit of the new tunnel (T2), distance 103.0-107.3 m, elevation 227.6-231.5 m (for location, see **Figure 6**).



Figure S26. Left wall of the main adit of the new tunnel (T2), distance 105.6-107.8 m, elevation 228.9-230.8 m (for location, see **Figure 6**).



Figure S27. Displacements of ice belts along a small ice wedge, right wall of the main adit of the new tunnel (T2), distance approximately 92.6-93.8 m, elevation 230.2-230.7 m (for location, see **Figure 6**).



Figure S28. Green grass, right wall of the main adit of the new tunnel (T2), distance 100.5 m, elevation 229.2 m (for location, see **Figure 6**).



Figure S29. Small ice wedge truncated by underground thermal erosion. Note small bodies of thermokarst-cave ice in the upper part of the photograph. Left wall of the main adit of the new tunnel (T2), distance 110.8-114.3 m, elevation 228.8-231.2 m (for location and interpretation, see **Figure 6**).



Figure S30. Ice wedges truncated by thermokarst and/or thermal erosion. Right wall of the main adit of the new tunnel (T2), distance 111.6-115.1 m, elevation 227.9-230.7 m (for location, see **Figure 6**).



Figure S31. Syngenetic ice wedge. Left wall of Crosscut #1 of the new tunnel (C1), distance 9.4-13.9 m, elevation 228.8-231.6 m (for location, see **Figure 10**).



Figure S32. Thermokarst-cave ice bodies above the ice wedge truncated by thermal erosion. Left wall of Crosscut #1 of the new tunnel (C1), distance 14.0-17.8 m, elevation 227.6-230.6 m (for location and interpretation, see **Figure 10**).



Figure S33. Organic-rich silt with micro-cryostructures and ice belts typical of undisturbed Yedoma. Note turbated organic-rich layers in Yedoma silt. Left wall of Crosscut #1 of the new tunnel (C1), distance 18.4-19.8 m, elevation 228.1-229.0 m (for location, see **Figure 10**).



Figure S34. Ice wedge truncated by thermal erosion and underground channels filled with thermokarst-cave ice and silt with inclusions of reworked organic matter. Right wall of Crosscut #1 of the new tunnel (C1), distance 16.4-18.0 m, elevation 229.0-230.2 m (for location and interpretation, see **Figure 10**).



Figure S35. Ice wedge cut by underground thermo-erosional channel. For details, see **Figures S36 and S37**. Right wall of Crosscut #1 of the new tunnel (C1), distance 22.1-26.0 m, elevation 228.7-231.6 m (for location and interpretation, see **Figure 10**).



Figure S36. Syngenetically frozen Yedoma silt with ice belts and micro-cryostructures and syngenetic ice wedge affected by underground thermal erosion. Right wall of Crosscut #1 of the new tunnel (C1), distance 24.5-25.5 m, elevation 228.9-229.7 m (for location, see **Figure 10**).



Figure S37. Syngenetically frozen Yedoma silt with ice belts and micro-cryostructures. Right wall of Crosscut #1 of the new tunnel (C1), distance 23.1-23.8 m, elevation 228.7-229.2 m (for location, see **Figure 10**).



Figure S38. Underground erosional channels filled with thermokarst-cave ice underlain by silt with reticulate-chaotic cryostructure. The channels started developing along ice wedges but eventually expanded and affected enclosing sediments. Left wall of Crosscut #1 of the new tunnel (C1), distance 27.0-28.6 m, elevation 228.2-229.4 m (for location and interpretation, see **Figure 10**).



Figure S39. Ice-wedge pseudomorph filled with sandy gravel. Left wall of Crosscut #1 of the new tunnel (C1), distance 42.2-46.1 m, elevation 228.3-231.5 m (for location, see **Figure 10**).



Figure S40. Ice wedge truncated by thermal erosion; underground channel filled with thermokarst-cave ice underlain by silt with reticulate-chaotic cryostructure. Right wall of Crosscut #1 of the new tunnel (C1), distance 29.0-30.8 m, elevation 228.3-230.7 m (for location, see **Figure 10**).



Figure S41. Thermokarst-cave ice underlain by silt with reticulate-chaotic cryostructure. Right wall of Crosscut #1 of the new tunnel (C1), distance 31.2-33.2 m, elevation 227.7-229.2 m (for location, see **Figure 10**).



Figure S42. Thermokarst-cave ice underlain by silt with reticulate-chaotic cryostructure (formed in the narrow underground channel developed along the ice wedge). Note turbated organic-rich layers in Yedoma silt. Right wall of Crosscut #1 of the new tunnel (C1), distance 33.7-35.3 m, elevation 227.9-229.1 m (for location, see **Figure 10**).



Figure S43. Pleistocene/Holocene boundary (thaw unconformity marked by truncated ice wedges and lenses). Right wall of Crosscut #1 of the new tunnel (C1), distance 41.0-44.0 m, elevation 228.8-231.0 m (for location and interpretation, see **Figure 10**).



Figure S44. Underground erosional channel filled with silt with reticulate-chaotic cryostructure; underlain by large thermokarst-cave ice body. Right wall of Crosscut #1 of the new tunnel (C1), distance 41.7-42.5 m, elevation 228.3-229.0 m (for location and interpretation, see **Figure 10**).